Deep–Sea Research I 202 (2023) 104190

Contents lists available at ScienceDirect

Deep-Sea Research Part I

journal homepage: www.elsevier.com/locate/dsri

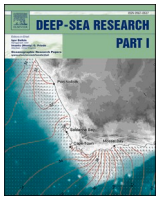

Phytoplankton carbon biomass: Insights from the eastern Indian Ocean

Shujin Guo [a,b,c], Feng Wang [a,d], Junhua Liang [a], Kangning Zhang [a,d], Xiaoxia Sun [a,b,c,d,*]

[a] Jiaozhou Bay National Marine Ecosystem Research Station, Institute of Oceanology, Chinese Academy of Sciences, Qingdao, 266071, PR China
[b] Laboratory for Marine Ecology and Environmental Science, Laoshan Laboratory, Qingdao, 266237, PR China
[c] Center for Ocean Mega-Science, Chinese Academy of Sciences, Qingdao, 266071, PR China
[d] University of Chinese Academy of Sciences, Beijing, 100049, PR China

ARTICLE INFO

Keywords:
Phytoplankton carbon
Physic-chemical parameters
Picophytoplankton
Utermöhl phytoplankton
C
Chl *a* ratio
Deep chlorophyll maximum
Eastern Indian Ocean

ABSTRACT

The study of phytoplankton carbon biomass is limited but has the potential to provide important insights into several oceanographic processes, such as the vertical carbon export and yield from the oceanic food web. In this study, we estimated the carbon biomass of the whole phytoplankton community in the eastern Indian Ocean (EIO) during spring of 2021 using flow cytometry and microscopy. We also examined the effect of physico-chemical parameters on the spatial distribution of phytoplankton carbon biomass (phytoplankton-C). In the EIO, the range of phytoplankton-C was between 0.03 and 33.96 μg C L^{-1}, with picophytoplankton (≤2 μm) accounting for 92.41 ± 8.95% and 89.06 ± 13.21% of the total phytoplankton-C in the surface and deep chlorophyll maximum (DCM) layer, respectively. Among various phytoplankton groups, *Prochlorococcus* and picoeukaryotes accounted for a major part of the phytoplankton-C in the EIO, contributing (57 ± 12%) and (25 ± 7%) to the depth-integrated carbon biomass, respectively. This was followed by *Synechococcus* (6 ± 4%), diatoms (6 ± 4%) and dinoflagellates (3 ± 1%). Phytoplankton-C exhibited significant variations in both horizontal and vertical distribution within the study area. Horizontally, the distribution of phytoplankton-C was markedly influenced by physical events in the EIO, such as freshwater inputs in the Bay of Bengal, Wyrtki Jet at the Equator and Southern Equatorial Current in the southern EIO. Vertically, different phytoplankton groups exhibited varying distribution patterns in carbon biomass with increasing depths, primarily due to their diverse responses to the vertical variation of irradiance and nutrients in the water column. The total phytoplankton-C in the surface layer (9.56 ± 3.01 μg C L^{-1}) and the DCM layer (9.07 ± 3.75 μg C L^{-1}) did not show a significant difference between each other (*t*-test, $p > 0.1$, n = 42), indicating that DCM didn't correspond to a phytoplankton-C maximum but rather a physiological adaptation of C: Chl *a* ratios of phytoplankton cells in the EIO. Therefore, vertical profiles of Chl *a* should be interpreted with caution when establishing their ecological significance in the study area. The carbon biomass of the entire phytoplankton community in the EIO was reported in this study, which could enhance our understanding of the contribution of different phytoplankton groups to the carbon pool and their role in the biogeochemical cycle in the EIO.

1. Introduction

As the primary producer in the ocean, phytoplankton can affect energy flow and material cycle (Graff et al., 2015). Therefore, understanding the distribution of phytoplankton biomass is essential for exploring the food web structure and material cycling in the ocean (Taylor and Landry, 2018). Phytoplankton cell abundance is a commonly used index to estimate phytoplankton biomass, but this method may not accurately represent the contribution of different-sized phytoplankton species, resulting in underestimation of larger species and overestimation of smaller ones (Harrison et al., 2015). Chlorophyll *a* (Chl *a*) concentration is another widely used index, but it can't provide information on the genus or species level of phytoplankton (Graff et al., 2015). Therefore, it is essential to develop a standardized method for estimating phytoplankton biomass, particularly in environments with diverse phytoplankton compositions, to better understand their contribution to oceanic processes such as energy flow and material cycling.

Phytoplankton cells play a crucial role in contributing to the particulate organic carbon in the ocean, and their organic carbon concentration is directly related to primary production and the global carbon

* Corresponding author. Jiaozhou Bay National Marine Ecosystem Research Station, Institute of Oceanology, Chinese Academy of Sciences, 7 Nanhai Road, Shinan District, Qingdao, 266071, PR China.
E-mail address: xsun@qdio.ac.cn (X. Sun).

https://doi.org/10.1016/j.dsr.2023.104190
Received 24 April 2023; Received in revised form 1 September 2023; Accepted 27 October 2023
Available online 30 October 2023
0967-0637/© 2023 Elsevier Ltd. All rights reserved.

cycle (Graff et al., 2015). Therefore, phytoplankton carbon (phytoplankton-C) is a useful parameter for expressing phytoplankton biomass in the study of marine ecosystems, providing insight into various oceanographic processes, including the vertical flux of organic matter, nutrient utilization patterns, and food web yield (Ara et al., 2019). Due to the inability to separate phytoplankton cells from other constituents such as zooplankton, heterotrophic bacteria, and detritus, direct measurement of phytoplankton-C in natural samples is not feasible. The most commonly used and practical method for measuring phytoplankton-C relies on cell counts and biovolume-carbon conversions based on empirical relationships (Menden-Deuer and Lessard, 2000; Sun and Liu, 2003; Harrison et al., 2015). Picophytoplankton (<2 μm) can be enumerated using a flow cytometer (Olson et al., 2018), while micro- and nonophytoplankton (≥2 μm) are typically counted using microscopy (Graff et al., 2015). This method allows for estimation of phytoplankton-C at the species and genus level and has been widely used in various oceanic regions (Jakobsen and Markager, 2016; Crawford et al., 2018).

The eastern Indian Ocean (EIO) is a region of great importance, providing food, natural resources, and other benefits to the surrounding countries (Hermes et al., 2019). It is subject to a range of physical events throughout the year. In the northern EIO, the Bay of Bengal receives freshwater inputs from rivers in its bordering countries and rainfalls, leading to near-surface stratification and the formation of a barrier layer (Jana et al., 2015). At the Equator, the Wyrtki Jet, a surface current generated by strong westerly winds in spring and fall, can be observed (Wyrtki, 1973). In the southern EIO, the Southern Equatorial Current (SEC) carries low-salinity water westward (Sardessai et al., 2010). Due to these factors, the ecosystem of the EIO is highly dynamic and variable (Phillips et al., 2021). Despite the importance of the EIO ecosystem to the surrounding countries, there have been few studies on the distribution of phytoplankton-C in this region, in contrast to the Atlantic and Pacific Oceans (Wang et al., 2013; Phillips et al., 2021). Previous research on phytoplankton biomass in the EIO has mainly relied on the determination of Chl *a* (Hong et al., 2012; Jiang et al., 2022) and phytoplankton cell abundance (Wei et al., 2019; Yuan et al., 2021; Chen et al., 2023), with sporadic studies on picophytoplankton carbon biomass (Wei et al., 2018; Chen et al., 2023). Study on the carbon biomass of the entire phytoplankton community is quite limited in the EIO. Therefore, the EIO has received less attention than other oceans in terms of phytoplankton-C, providing little information for understanding the role of phytoplankton played in the biogeochemical cycle (especially carbon cycle) in this region.

The deep chlorophyll maximum (DCM) is a common characteristic of phytoplankton vertical distribution in the stratified waters of the EIO. It is typically lies just below the mixed layer and coincides with the top of the nutricline (Jiang et al., 2022), with depth ranging from 50 m to 90 m (Hong et al., 2012; Jiang et al., 2022). The DCM is a significant contributor to the integrated Chl *a* in the EIO, with estimates indicating that it can account for up to 70% of the total Chl *a* (Hong et al., 2012). Various processes contribute to the formation of a DCM (Pérez et al., 2006). These encompass the passive accumulation of cells at a pycnocline, or the behavioral aggregation of motile cells as a defense mechanism against grazing (Hodges and Rudnick, 2004). DCM may not necessarily correspond to a surge in biomass, but can also indicate a physiological adjustment of the cellular carbon-to-chlorophyll *a* (C: Chl *a*) ratio (Hanson et al., 2007). In practical situations, a decline in the C: Chl *a* ratio was occasionally observed with diminishing ambient irradiance (i.e. with increasing depth) due to the cells adapting to lower light levels (Pérez et al., 2006). This phenomenon, known as photoacclimation, often occurs just beneath the mixed layer. In the EIO, whether the DCM represents a phytoplankton carbon biomass layer remains unclarified. Limited research has been conducted to investigate the vertical distribution of phytoplankton-C in the EIO until now, mainly due to the laborious nature of microscopy techniques, which restricts our understanding of the ecological importance of the DCM. This lack of information limits our ability to assess the DCM's ecological significance, such as its role as a food source for zooplankton and its contribution to primary production and carbon export.

In this study, we aimed to comprehensively investigate the phytoplankton carbon biomass and its distribution in the EIO during the spring of 2021. By using multidisciplinary methods, we were able to determine the carbon biomass of the entire phytoplankton community and examine its spatial distribution and the factors that regulate it. Furthermore, we analyzed the contributions of different phytoplankton groups (*Prochlorococcus*, *Synechococcus*, picoeukaryotes, diatoms and dinoflagellates) to the total phytoplankton carbon biomass, and investigated their vertical distribution patterns and associated physical and chemical factors. Finally, we investigate whether the DCM is a carbon biomass maximum for phytoplankton in the EIO. This study will contribute to a better understanding of the phytoplankton carbon biomass and its role in the biogeochemical cycle, particularly the carbon cycle, in the EIO.

2. Materials and methods

2.1. Study area and sampling stations

This cruise was conducted onboard the R/V *Shiyan III* from April 26 to June 2, 2021, covering the EIO region between 15°N and 10°S and 80°E and 95°E, as shown in Fig. 1. A total of 42 stations were established, and four transects were divided, including two longitudinal ones (Section E87 and E80) and two latitudinal sections (Section EQ and S10). Section E87 covered 16 stations (15°N~8°S) along 87°E, and section E80 covered 7 stations (2°N~5°S) along 80°E. Section EQ included 7 stations along the equator from 82°E to 93°E, and section S10 included 5 stations (87°E~93.8°E) along 10°S. Seawater samples were collected from all 42 stations for further analysis.

2.2. Sampling and analysis

2.2.1. Environmental parameters

At each of the 42 stations, seawater samples were collected from seven different depths (5 m, 25 m, 50 m, 75 m, 100 m, 150 m, and 200 m) within the upper 200 m of the water column using 12-L Niskin bottles equipped with a Sea-Bird CTD (Conductivity, Temperature and Depth; SBE 19 Plus) rosette sampler. In addition, one water sample was collected from the depth of DCM (Table S1), which was determined by the maximal fluorescence detected by a CTD-mounted fluorometer. The CTD was also used to measure temperature and salinity. Samples for dissolved inorganic nutrient analysis were collected at each layer and filtered through a 0.45 μm pore-size cellulose acetate membrane. The filtered samples were stored in - 20 °C until analysis. The filtrates were processed in the lab and analyzed with a Technicon AA3 auto-analyzer (Bran-Lube, GmbH) (Han et al., 2012). The detection limit for nutrients were 0.02 μmol L^{-1} for NO_3^-, 0.01 μmol L^{-1} for NO_2^-, 0.01 μmol L^{-1} for NH_4^+, 0.01 μmol L^{-1} for PO_4^{3-} and 0.10 μmol L^{-1} for SiO_3^{2-}. For Chl *a* analysis, 500 mL samples were filtered through 0.7 μm Whatman GF/F filters, and then extracted in 90% acetone for 24 h in the dark at 4 °C. Chl *a* concentrations were determined using a Turner Design fluorometer (Turner Designs Model 10) following the method described by Welschmeyer (1994).

2.2.2. Phytoplankton analysis

Samples for large-sized phytoplankton (>2 μm) were fixed with formaldehyde solution (2% final concentration) in polyethylene bottles aboard. In the lab, the samples were analyzed with the classical Utermöhl method (Paxinos and Mitchell, 2000). A 100 mL sample was allowed to settle in sedimentation chambers (Hydrobios, Kie, Germany) for 24–48 h, and phytoplankton cells were then identified and counted with an inverted microscope at 200 × and 400× magnification (Paxinos and Mitchell, 2000). The linear dimensions of phytoplankton cells were

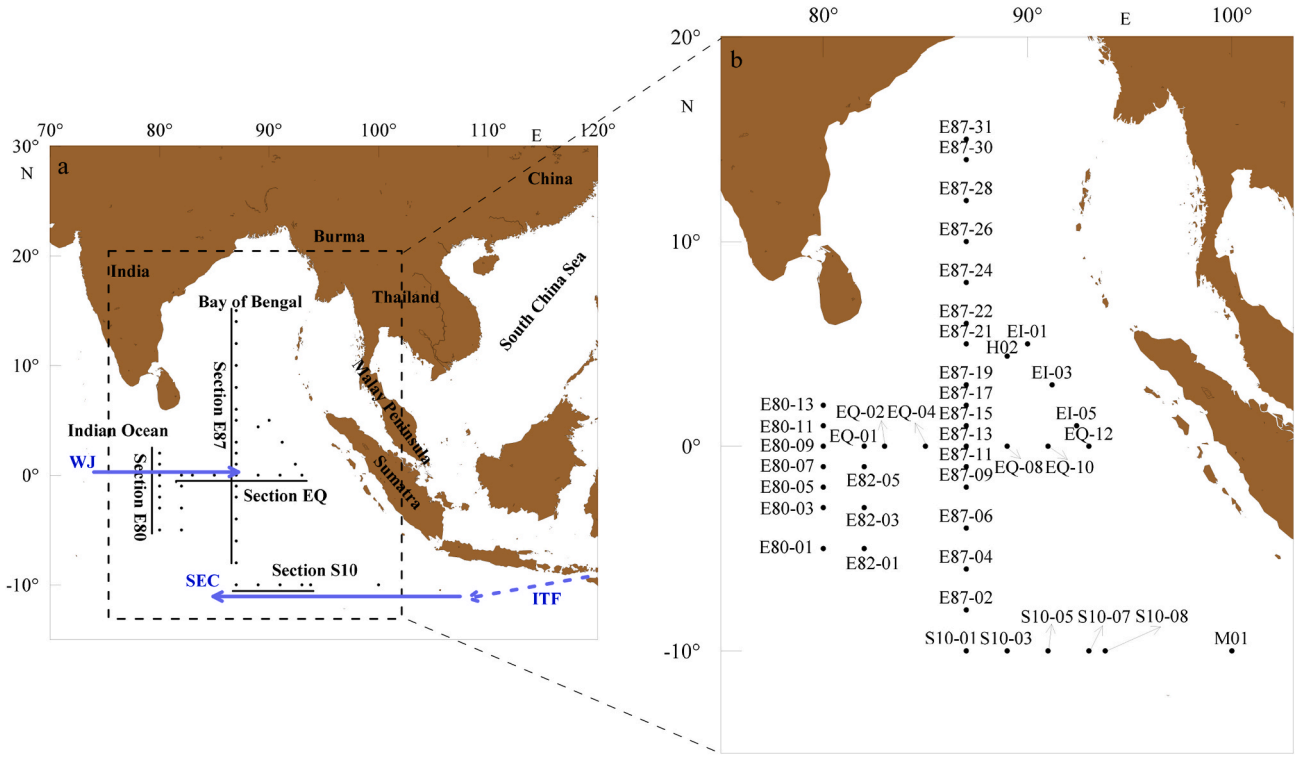

Fig. 1. Sampling stations in the EIO during spring, 2021. a: general view of the study area and sampling stations; b: enlarged view of the sampling stations. The blue arrows indicate the current system (WJ: Wyrtki Jet, SEC: South Equatorial Current, ITF: Indonesia Throughflow).

measured with a micrometer under the microscope, and the volume of each phytoplankton species was then calculated from measured dimensions by assigning an appropriate geometrical shape (Hillebrand et al., 1999). For each phytoplankton species, at least twenty five cells were measured for their linear dimension. The phytoplankton-C was calculated using the conversion equation:

$$PC = a \times V^b \quad (1)$$

where PC is phytoplankton-C, V is cell volume, a and b are 0.288 and 0.811 for diatoms, and 0.216 and 0.939 for dinoflagellates and other phytoplankton groups, respectively (Menden-Deuer and Lessard, 2000; Crawford et al., 2018; Taylor and Landry, 2018).

4.5 mL samples for picophytoplankton (≤2 μm) analysis were collectd and fixed with buffered paraformaldehyde (final concentration of 0.5%), placed at room temperature for 10 min, and then frozen in liquid nitrogen at −80 °C aboard. After returning to the lab, samples were analyzed with a flow cytometry (FCM) (Becton and Dickinson). 600 μL sample was mixed with 20 μL yellow-green fluorescent beads (diameter = 1 μm, Polysciences) as the internal standard (Olson et al., 2018). Three groups of picophytoplankton [*Prochlorococcus* (PRO), *Synechococcus* (SYN) and picoeukaryotes (PEUK)] were distinguished and enumerated according to their side scattering, and orange and red fluorescence (Fig. S1). The picophytoplankton carbon biomass (picophytoplankton-C) was calculated using the conversion factor of Zamanillo et al. (2019): 175 fg C cell^{-1} for SYN, 51 fg C cell^{-1} for PRO and 1319 fg C cell^{-1} for PEUK. It should be noted that uncertainty sources for the carbon estimation in this study were cell biovolume estimates and conversion factors.

2.3. Data analysis and statistical methods

The depth-integrated carbon biomass of phytoplankton in the water column was calculated using the trapezoidal integral method:

$$DC = \sum_{n}^{n+1} \frac{(C_i + C_{i+1})}{2} \times (D_{i+1} - D_i) \quad (2)$$

where DC represents the depth-integrated carbon biomass of phytoplankton, C_i represents the carbon biomass of phytoplankton in layer i, D_i represents the depth of layer i, and n represents the sampling level.

The dominance index (Y) of phytoplankton species was calculated according to the formula:

$$Y = \frac{n_i}{N} \times f_i \quad (3)$$

where n_i is the sum of species i's cell abundance in all the samples; N is the sum of all the species cell abundances, and f_i is the species i occurrence frequency in all the samples.

The spatial distribution of temperature, salinity, nutrients, and phytoplankton data was visualized using the Golden Software Surfer 11. The vertical distribution pattern of phytoplankton and Chl *a* data was visualized using the Golden Software Grapher 8. OriginPro 8.5 was used to draw the scatter plot of phytoplankton carbon biomass and Chl *a*. Pearson Correlation Analysis was used to analyze the relationship between phytoplankton carbon biomass and environmental parameters using software SPSS14.0. T-test was used to verify the significant difference between two groups of data with the significance level being set at $p < 0.05$.

3. Results

3.1. Hydrological conditions in the EIO

During the cruise, the EIO showed distinct horizontal variation in hydrological conditions. The surface temperature ranged from 28.00 to 31.65 °C (with a mean of 29.95 ± 0.87 °C), being highest in the Bay of Bengal and decreasing southwards (Fig. 2a). The surface salinity ranged from 31.83 to 34.87 (mean = 34.09 ± 0.79) and the lowest value

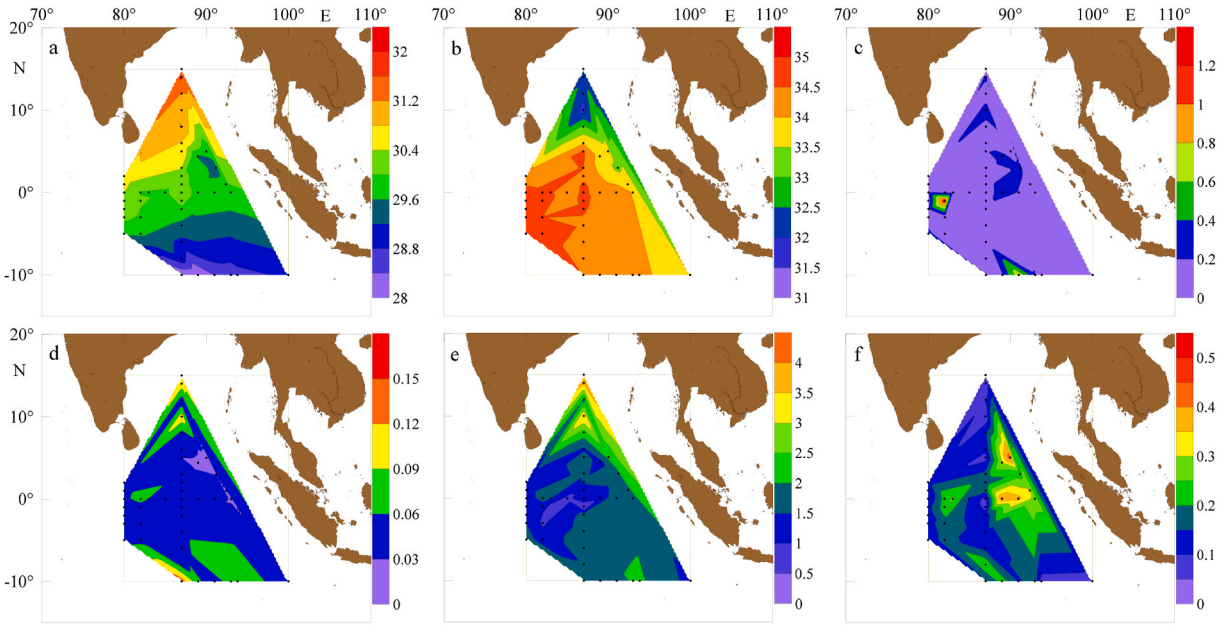

Fig. 2. Horizontal distributions of temperature (a, °C), salinity (b), DIN (NO_3-N + NO_2-N + NH_4-N) (c, μmol L^{-1}), phosphate (d, μmol L^{-1}), silicate (e, μmol L^{-1}) and Chl *a* (f, μg L^{-1}) in the surface layer in the EIO.

appeared in the Bay of Bengal (Fig. 2b). Notably, a surface warm tongue with high salinity (>34) was observed in the equatorial region, moving from west to east between 80°E and 88°E, indicating the influence of the Wyrtki Jets (Wang, 2017). DIN ranged from 0.07 to 1.18 μmol L^{-1} in the surface layer, with the highest value appearing in the western equatorial region (Fig. 2c). Phosphate and silicate concentrations ranged from 0.02 to 0.14 μmol L^{-1} and 0.41 to 3.95 μmol L^{-1}, respectively, with both showing high values in the Bay of Bengal and decreasing southward (Fig. 2d and e). However, sporadic high nutrient values were observed in the Section S10 (Fig. 2c-e). The Chl *a* concentration ranged from 0.06 to 0.43 μg L^{-1}, with a scattered distribution pattern in the surface layer (Fig. 2f).

Table 1 presents the mean environmental parameters for each layer, and Fig. 3 shows the vertical distributions of these parameters along four sections. The vertical profiles demonstrate the typical pattern of the oligotrophic ocean in the EIO. The water columns were found to be stratified due to high temperatures in the upper layer (Fig. 3a-d). This pronounced stratification led to depleted nutrient concentrations in the upper layer, with nutrient levels increasing rapidly from 100 to 200 m (Fig. 3i-p). A deep nutrient-cline was observed around 100 m depth in most parts of the EIO (Fig. 3i-k), except for Section S10 in the southern EIO (Fig. 3l), where the deep nutrient-cline appearing around 50 m depth. The DIN: PO_4^{3-} in the upper layer (mostly <8 in the top 50 m) was much lower than in deeper layers (Fig. 3q-t), indicating a severe nitrogen limitation in the upper layer in the EIO. The vertical distribution of Chl *a* concentration showed a DCM in the EIO, located at a depth of 50~100 m, and then steadily decreased from the DCM layer down to the 200 m layer (Fig. 3y-B). The Chl *a* concentration ranged from 0.07 to 0.77 μg L^{-1} in the DCM layer. Concentrations of ≤0.20 μg L^{-1} were most frequently found in the surface layer (80% frequency), while levels of 0.4-0.7 μg L^{-1} were most common in the DCM layer (76% frequency).

3.2. Phytoplankton cell abundance and species composition in the EIO

For Utermöhl phytoplankton, a total of 173 species belonging to 4 classes and 52 genera were identified. Among these, diatoms and dinoflagellates emerged as the most prominent groups. Diatoms, specifically, constituted a substantial portion of the Utermöhl phytoplankton community, with 30 genera and 72 species identified. These diatom species accounted for 41.60% of the overall species richness. On the other hand, dinoflagellates exhibited a diverse presence, with 19 genera and 96 species identified, contributing to 55.49% of the total species richness. Dominant phytoplankton species were shown in Table S2. Notably, the diatom species *Pseudo-nitzschia delicatissima* stood out as the most dominant phytoplankton species in the study area, further accentuating the significance of diatoms within the Utermöhl phytoplankton community. The Utermöhl phytoplankton exhibited a wide range of cell abundance, spanning from 0 to 7800.00 cells L^{-1}, with a mean value of 221.10 ± 619.67 cells L^{-1}. Within this phytoplankton community, diatoms displayed a cell abundance range of 0 to 7656.00 cells L^{-1}, with a mean of 162.40 ± 587.73 cells L^{-1}. Remarkably, diatoms constituted 62 ± 35% of the overall Utermöhl phytoplankton cell

Table 1
Summary statistics of environmental factors (mean ± standard deviation) at different depths in the EIO.

Depth/m	Temperature/°C	Salinity	DIN/(μmol L^{-1})	Phosphate/(μmol L^{-1})	Silicate/(μmol L^{-1})	DIN/PO_4^{3-}	Chl *a*/(μg L^{-1})	Phytoplankton-C/(μg C L^{-1})
5	29.95 ± 0.87	34.09 ± 0.79	0.19 ± 0.19	0.05 ± 0.02	1.68 ± 0.70	4.49 ± 5.43	0.16 ± 0.09	9.56 ± 3.00
25	29.81 ± 0.66	34.16 ± 0.67	0.19 ± 0.03	0.05 ± 0.03	1.59 ± 0.58	5.19 ± 7.38	0.19 ± 0.09	10.37 ± 4.84
50	28.89 ± 2.29	34.41 ± 0.49	1.12 ± 3.14	0.16 ± 0.28	3.06 ± 4.32	5.09 ± 4.74	0.29 ± 0.10	10.50 ± 2.46
75	26.26 ± 4.25	34.57 ± 0.39	4.77 ± 6.43	0.49 ± 0.48	7.42 ± 8.29	6.29 ± 4.20	0.39 ± 0.15	8.29 ± 3.36
DCM	26.84 ± 3.20	34.67 ± 0.38	3.25 ± 4.73	0.42 ± 0.38	5.94 ± 6.45	6.24 ± 4.76	0.46 ± 0.13	9.07 ± 3.75
100	23.10 ± 3.33	34.93 ± 0.28	9.79 ± 6.38	0.97 ± 0.42	11.48 ± 7.91	9.17 ± 3.18	0.26 ± 0.11	3.94 ± 2.15
150	17.48 ± 2.02	35.00 ± 0.23	18.27 ± 4.86	1.56 ± 0.31	19.42 ± 7.24	11.66 ± 1.53	0.05 ± 0.06	0.61 ± 0.36
200	14.23 ± 1.06	35.01 ± 0.17	23.59 ± 4.12	1.86 ± 0.27	25.26 ± 6.39	12.70 ± 1.26	0.01 ± 0.01	0.33 ± 0.44

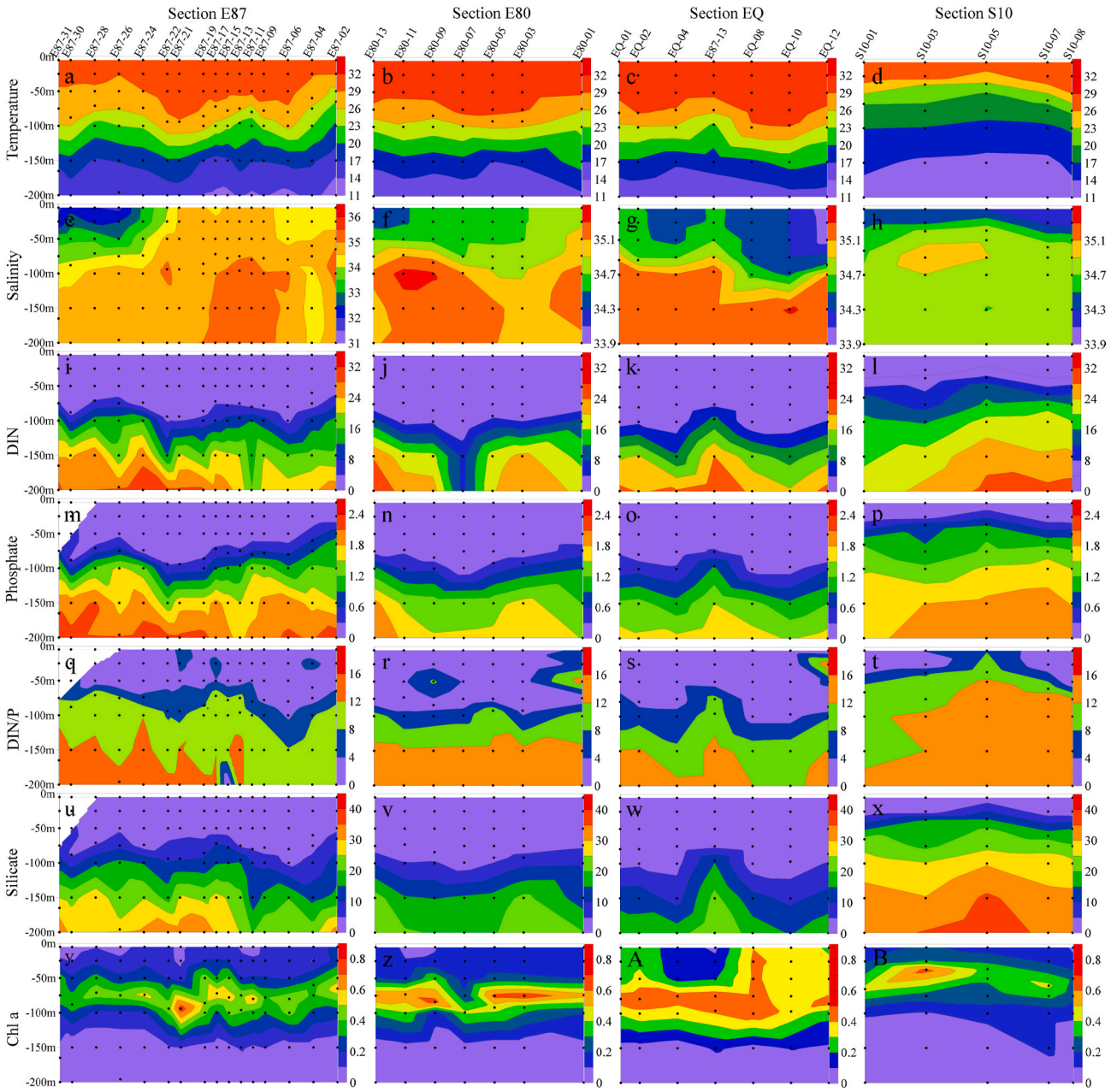

Fig. 3. Vertical profile for temperature (a-d, °C), salinity (e-h), DIN (i-l, μmol L^{-1}), phosphate (m-p, μmol L^{-1}), DIN/PO_4^{3-} (q-t), silicate (u-x, μmol L^{-1}) and Chl *a* (y-B, μg L^{-1}) along section E87, E80, EQ and S10 in the EIO.

abundance. In the case of dinoflagellates, their cell abundance varied from 0 to 144.00 cells L^{-1} with a mean value of 25.18 ± 28.14 cells L^{-1}, accounting for 25 ± 30% of the total Utermöhl phytoplankton cell abundance.

Picophytoplankton exhibited a broader range in cell abundance, from 0 to 258011 cells mL^{-1}, with a mean of 79078 ± 69799 cells mL^{-1}. Among the various picophytoplankton groups, PRO demonstrated the highest cell abundance, ranging from 150 to 254377 cells mL^{-1} with a mean of 75881 ± 68122 cells mL^{-1}. This group contributed significantly, representing 87 ± 17% of the total picophytoplankton cell abundance. Following PRO, SYN exhibited a cell abundance range of 0 to 34533 cells mL^{-1}, with a mean of 2301 ± 3674 cells mL^{-1}, accounting for 9 ± 15% of the total picophytoplankton cell abundance. Lastly, PEUK had the smallest contribution, ranging from 0 to 11283 cells mL^{-1}, with a mean of 1171 ± 1435 cells mL^{-1}, making up 3 ± 6% of the total picophytoplankton cell abundance. For a visual representation of the distribution patterns of both Utermöhl phytoplankton and picophytoplankton cell abundance in the study area, please refer to Figs. S2–4.

3.3. Horizontal distributions of phytoplankton carbon biomass in the EIO

In this study, phytoplankton-C ranged from 0.03 to 33.96 μg C L^{-1} for samples of all depths in the whole study area. In the surface layer of all stations, phytoplankton-C ranged from 4.70 to 18.85 μg C L^{-1} (mean = 9.56 ± 3.01 μg C L^{-1}) (Fig. 4a). In the Bay of Bengal, this value varied from 5.75 to 6.52 μg C L^{-1}. At the Equator, the surface phytoplankton-C was relatively high at stations E80-13, E80-07, EQ-01, EQ-04, and E87-13, where phytoplankton-C exceeded 10 μg C L^{-1}. However, in the eastern Equator region, phytoplankton-C decreased to around 7 μg C L^{-1}. Another relatively high phytoplankton-C value was observed in the southern EIO. In Section S10, the surface phytoplankton-C exceeded 10 μg C L^{-1} at stations S10-01, S10-03, S10-05 and S10-07, with the highest

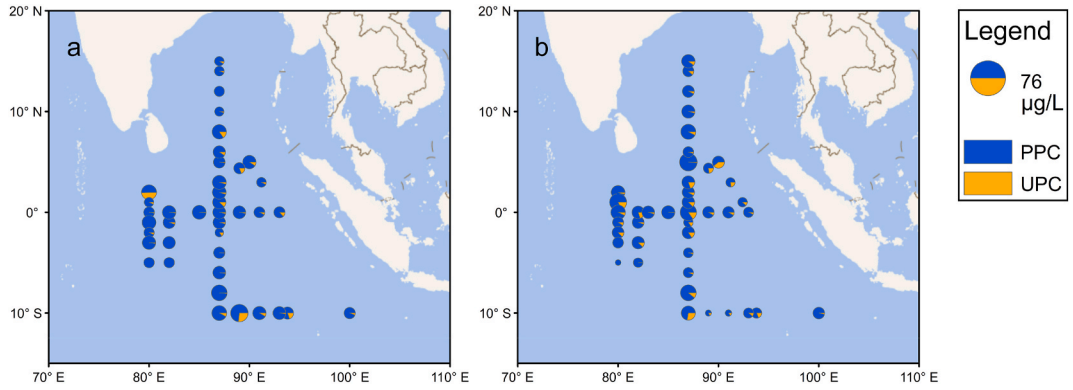

Fig. 4. Horizontal distributions of phytoplankton-C (μg C L^{-1}) in the surface layer (a) and the DCM layer (b) in the EIO during spring, 2021. a: surface layer; b: DCM layer. PPC, picophytoplankton carbon; UPC, Utermöhl phytoplankton carbon.

value reaching 13.83 μg C L^{-1} at station S10-01.

Picophytoplankton (≤2 μm) was the most dominant group in terms of carbon biomass, accounting for 50-98% (mean = 92.41 ± 8.95%) of total phytoplankton-C in the surface layer, while the contribution of larger Utermöhl phytoplankton (size >2 μm) was minor, representing 0-37% (mean = 7.59 ± 8.95%) of the total phytoplankton-C (Fig. 4a). In the DCM layer, phytoplankton-C ranged from 1.97 to 19.25 μg C L^{-1} (mean = 9.07 ± 3.75 μg C L^{-1}), with picophytoplankton-C and Utermöhl phytoplankton-C accounting for 32-99% (mean = 89.06 ± 13.21%) and 0-68% (mean = 11 ± 13%) of total phytoplankton-C, respectively (Fig. 4b). No significant difference was observed for phytoplankton-C between the surface layer and the DCM layer (*t*-test, $p > 0.05$, n = 42).

The contributions of picophytoplankton-C to the total phytoplankton-C across various regions within the EIO were presented in Fig. 5. In the surface layer, the ratios of picophytoplankton-C to total phytoplankton-C was highest in the Bay of Bengal (95.55%) and the equatorial Indian Ocean (94.40%), respectively. Following closely was the western part of the EIO (90.19%), while the southern part of the EIO displayed the comparatively lower yet significant value of 88.14%. In the DCM layer, picophytoplankton-C/phytoplankton-C in the Bay of Bengal, the equatorial Indian Ocean, and the western portion of the EIO maintained similar proportions of 91.69%, 90.97%, and 91.98%, respectively. The southern sector of the EIO demonstrated a relatively diminished value of 83.13%. Irrespective of the specific region or layer, picophytoplankton-C consistently represented a substantial fraction, surpassing 80% of the entire phytoplankton-C content in the study area.

The depth-integrated phytoplankton-C in the study area ranged from 601.69 to 1812.36 mg C m^{-2} (mean = 1105.38 ± 259.48 mg C m^{-2}) (Fig. 6). Of the various groups, PRO contributed the most to the depth-integrated carbon biomass, ranging from 286.52 to 1161.31 mg C m^{-2} (mean = 626.95 ± 168.19 mg C m^{-2}), accounting for 57 ± 12% of the total depth-integrated carbon biomass. This was followed by PEUK, which accounted for 25 ± 7% of the total depth-integrated carbon biomass. The contribution of other groups were similar, with SYN, diatoms and dinoflagellates accounting for 6 ± 4%, 6 ± 4% and 3 ± 1% of the total depth-integrated carbon biomass, respectively. Generally, PRO and PEUK accounted for a significant proportion of the total phytoplankton-C in the EIO.

3.4. Vertical distributions of phytoplankton carbon biomass in the EIO

The distributions of phytoplankton carbon biomass along four transects are shown in Fig. 7, and the vertical distributions of carbon biomass for different phytoplankton groups are presented in Fig. 8. Phytoplankton-C was relatively high in the upper 100 m layer, and then

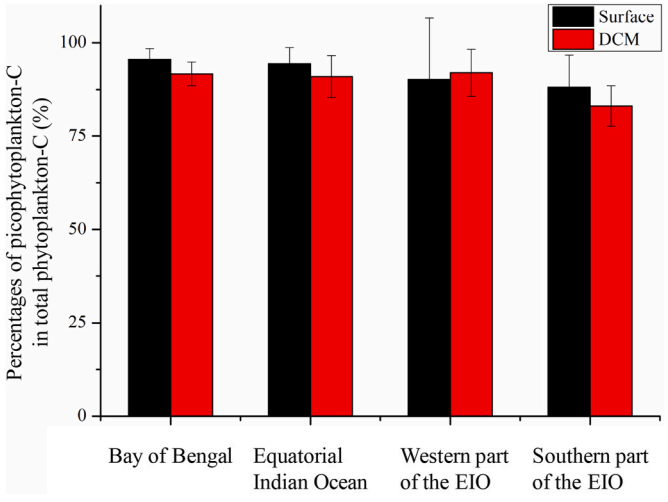

Fig. 5. Percentages of picophytoplankton-C in total phytoplankton-C in the surface and DCM layer in different regions in the EIO. Bay of Bengal: including stations E87-31, E87-30, E87-28 and E87-26; equatorial Indian Ocean: including stations EQ-01, EQ-02, EQ-04, EQ-08, EQ-10 and EQ-12; western part of the EIO: including stations E80-01, E80-03, E80-05, E80-07, E80-09, E80-11 and E80-13; southern part of the EIO: including stations M01, S10-09, S10-07, S10-05, S10-03 and S10-01.

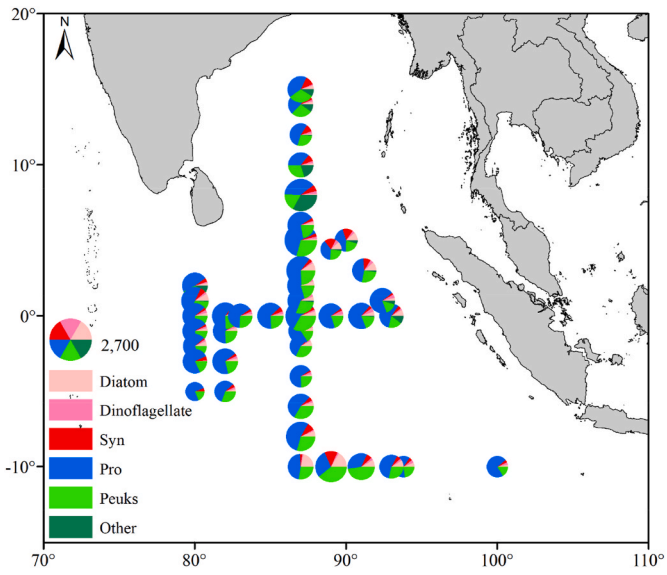

Fig. 6. Depth-integrated carbon biomass (mg C m^{-2}) of phytoplankton carbon including PRO, PEUK, SYN, diatoms, dinoflagellates and others in the study area.

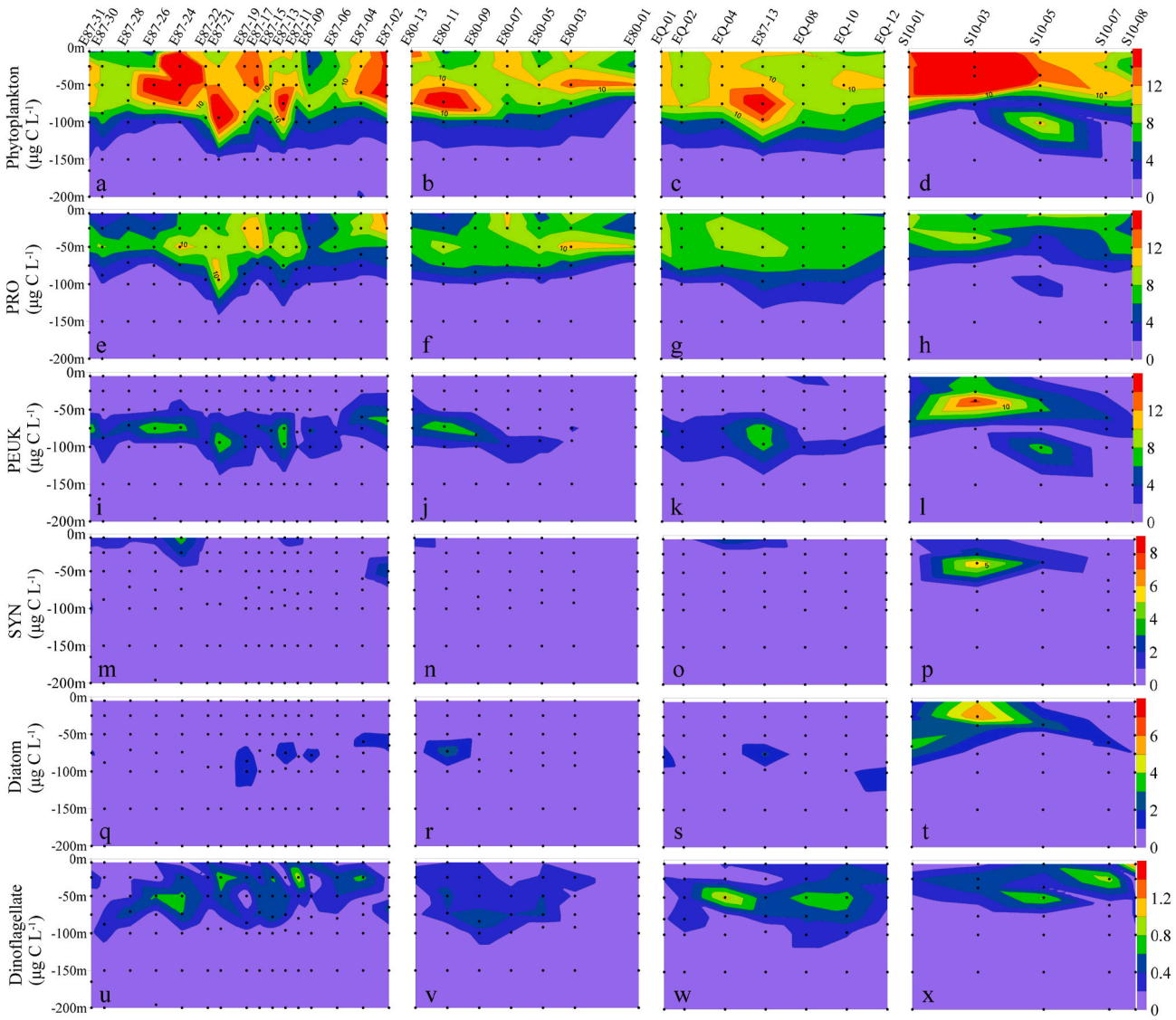

Fig. 7. Sectional distributions of total phytoplankton-C (a-d), PRO-C (e-h), PEUK-C (i-l), SYN-C (m-p), diatom-C (q-t) and dinoflagellate-C (u-x) in the study area.

rapidly decreased as water depth increased (Fig. 7a-d). The distribution pattern of PRO-C (Fig. 7e-h) was similar to that of total phytoplankton-C, with a nearly homogenous distribution in the upper 50 m layer, and subsequently decreasing from the DCM layer downwards (Fig. 8a). PEUK showed a different distribution pattern from PRO, with high values being concentrated between 50~100 m (Fig. 7i-l). The box-whisker plot also indicated that PEUK was highest in the DCM layer (Fig. 8b). SYN-C was lower than PRO and PEUK, and it mostly concentrated in the upper 50 m layer (Fig. 7m-p), gradually decreasing with increasing water depth (Fig. 8c). As the most dominant Utermöhl phytoplankton groups, diatom and dinoflagellate showed different distribution patterns. Diatom-C concentration was usually low in the upper 50 m, and high values concentrated around 50~100 m, except for a significant value in the upper layer of station S10-03 (Fig. 7q-t). The box-whisker plot showed that diatom carbon was highest in the DCM layer (Fig. 8d). Dinoflagellates, in contrast, were distributed homogenously in the upper 50 m layer (Fig. 7u-x, Fig. 8e). In general, different phytoplankton groups showed different vertical distribution patterns in carbon biomass.

The vertical distribution of total phytoplankton-C and Chl *a*, as well as the C: Chl *a* values of phytoplankton in the study area, are compared in Fig. 9. The concentration of phytoplankton-C was homogenous in the layers above the DCM, gradually decreasing downwards (Fig. 9a). Chl *a* concentrations, however, increased from the surface to DCM layer and then decreased downward (Fig. 9b). Hence, the DCM did not reflect the maximum in phytoplankton carbon biomass in the study area. The C: Chl *a* ratios of phytoplankton ranged from 20.28 to 132.16 g g^{-1} (mean = 70.34 ± 28.52 g g^{-1}) in the surface layer, which was significantly higher than that in the DCM (ranging 3.62~34.90 g g^{-1}, mean = 19.63 ± 6.86 g g^{-1}) (*t*-test, $p < 0.05$, n = 42), and the ratio decreased from the surface to the DCM layer before remaining essentially constant from the DCM layer downwards (Fig. 9c).

3.5. Pearson correlation analysis (PCA)

Pearson correlation analysis (PCA) was conducted between phytoplankton carbon biomass and various environmental parameters in the EIO (Table 2). PRO showed a significantly positive correlation with temperature and a negative correlation with depth, DIN, PO_4^{3-} and SiO_3^{2-}. In contrast, PEUK exhibited a significant negative correlation with temperature and a positive correlation with depth, DIN, PO_4^{3-} and SiO_3^{2-}. The SYN was significantly and negatively correlation with salinity and depth, although no significant correlation was observed between SYN and nutrients. Diatom and dinoflagellate showed different correlations

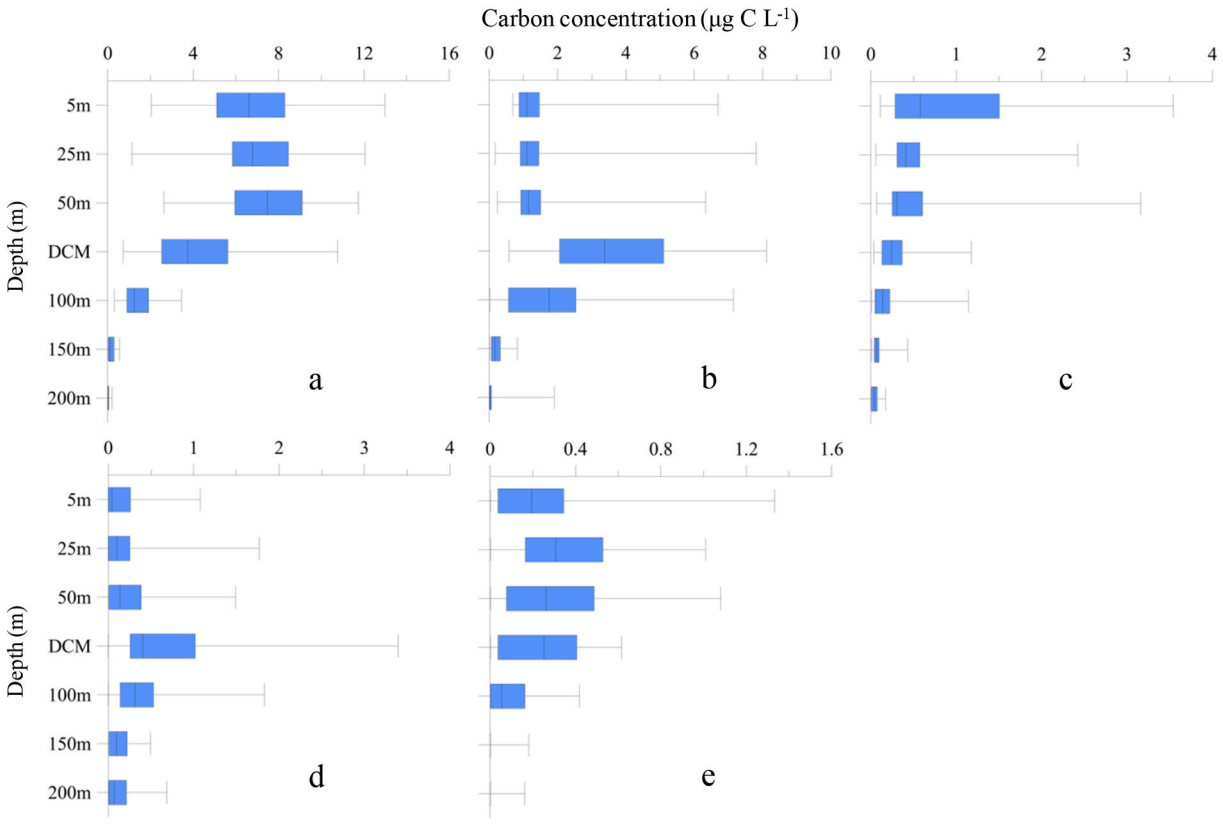

Fig. 8. Vertical distributions of PRO-C (a), PEUK-C (b), SYN-C (c), diatom-C (d) and dinoflagellate-C (e) in the EIO. Box plots show the median value (mid-line), the 25% and 75% quantiles (box), and the 5 and 95% quantiles (whiskers).

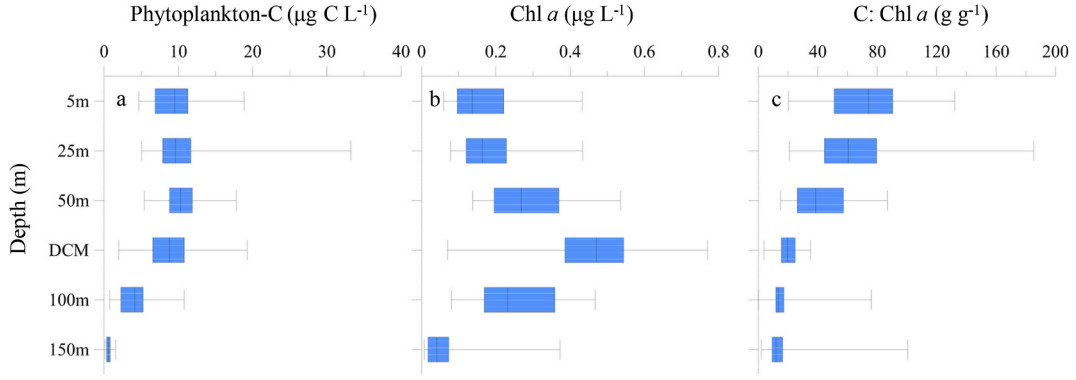

Fig. 9. Vertical profiles of phytoplankton-C (a, μg C L^{-1}), Chl *a* (b, μg L^{-1}) and C: Chl *a* ratio (c, g g^{-1}) of phytoplankton in the EIO. Box plots show the median value (mid-line), the 25% and 75% quantiles (box), and the 5 and 95% quantiles (whiskers).

Table 2
Pearson correlation analysis (R values) between the phytoplankton-C (μg C L^{-1}) (including total phytoplankton and various phytoplankton groups including PRO, PEUK, SYN, diatom and dinoflagellate) and environmental parameters in the upper 100 m layer in the EIO.

	Temperature (°C)	Salinity	Depth (m)	DIN (μ mol L^{-1})	PO_4^{3-} (μ mol L^{-1})	SiO_3^{2-} (μ mol L^{-1})
Total phytoplankton	0.31**	-0.14*	-0.37**	-0.35**	-0.34**	-0.24**
PRO	0.59**	-0.13**	-0.59**	-0.55**	-0.61**	-0.49**
PEUK	-0.28**	0.22**	0.27**	0.15*	0.25**	0.25**
SYN	0.13	-0.33**	-0.36**	-0.13	-0.10	-0.06
Diatom	-0.22**	0.12	0.11	0.10	0.17*	0.17*
Dinoflagellate	0.26**	-0.10	-0.23**	-0.25**	-0.31**	-0.23**

*$p < 0.05$ (2-tailed).
**$p < 0.01$ (2-tailed).

with environmental parameters, with diatoms positively correlated with PO_4^{3-} and SiO_3^{2-} and dinoflagellates negatively correlated with depth, DIN, PO_4^{3-} and SiO_3^{2-}. Consequently, various phytoplankton groups exhibited unique correlations with environmental parameters in the EIO.

4. Discussion

In order to obtain depth-resolved phytoplankton carbon biomass in the EIO that could serve as a common currency for understanding carbon transformations between trophic levels and vertical carbon fluxes, two independent and complementary methods (FCM and microscopy) were combined. The resulting dataset provides unique measurements of phytoplankton carbon biomass in the euphotic zone of the EIO, which are valuable for assessing carbon flows from primary producers to other trophic levels, as well as remineralized and export production in the EIO.

4.1. Phytoplankton carbon biomass dominated by picophytoplankton in the EIO

Total phytoplankton-C ranged 0.03 to 33.96 μg C L^{-1} in the EIO in this study, which is lower than levels reported in several coastal seas, such as York River estuary (140 to 1640 μg C L^{-1}) (Ray et al., 1989), Apalachicola Bay (18 to 1985 μg C L^{-1}) (Putland and Iverson, 2007), and similar with that reported in several oligotrophic regions, such as the Atlantic subtropical gyres (4 to 20 μg C L^{-1}) (Pérez et al., 2006), the equatorial Pacific Ocean (4 to 58 μg C L^{-1}) (Graff et al., 2015) and the oligotrophic Mediterranean Sea (5 to 40 μg C L^{-1}) (Mena et al., 2019).

Picophytoplankton dominated the photic zone in terms of carbon biomass, accounting for 92.41 ± 8.95% and 89.06 ± 13.21% of the total phytoplankton carbon biomass in the surface and DCM layer, respectively (Figs. 4 and 5). This dominance can be attributed to the small cell sizes and large surface areas per unit volume of picophytoplankton cells, which enables them to efficiently acquire nutrients for growth in oligotrophic conditions, giving them an advantage over larger phytoplankton cells (Marañón et al., 2012). Large-sized phytoplankton cells, on the other hand, are more easily limited by nutrient availability (Mena et al., 2019). The environmental conditions in the EIO during this study were typical of a stratified and oligotrophic region, with extremely low nutrient levels in the upper layers (Fig. 3). As a result, picophytoplankton had a competitive advantage over larger-sized phytoplankton, leading to their dominance in carbon biomass in this region. Since ecological functions vary among different sizes of phytoplankton, with larger-sized cells being prone to grazing by mesozooplankton and smaller-sized ones being more easily recycled in the euphotic zone due to their low sinking velocities (Taylor and Landry, 2018), the dominance of picophytoplankton in the EIO might indicate a promoted microbial loop in this area (Yuan et al., 2021).

Among the different phytoplankton groups in the EIO, PRO contributed 57 ± 12% to the depth-integrated carbon biomass, followed by PEUK at 25 ± 7%, while the other phytoplankton groups contributed less than 20% (Fig. 6). Therefore, PRO was the most dominant phytoplankton group in the region in terms of carbon. This finding is consistent with a study in the Pacific Ocean, which reported that PRO accounted for 65% of the total phytoplankton carbon biomass (Blanchot and Rodier, 1996). Although PEUK and SYN have larger cellular sizes than PRO (Yuan et al., 2021), they exhibited cell abundance that were approximately 1-2 orders of magnitude lower than that of PRO in this study (Fig. S3), which contributed to PRO's dominant position in carbon biomass in the EIO.

4.2. The impact of physical events on the horizontal distribution of phytoplankton-C in the EIO

This study revealed contrasting hydrographic characteristics across the northern to southern EIO driven by different physical events. Despite consistent nutrient depletion with PRO dominance, variations in phytoplankton-C concentrations were also observed in the surface layer (Fig. 4a). For example, in the Bay of Bengal, low salinity in the surface layer at stations E87-31, E87-30 and E87-28, resulting from freshwater inputs (Fig. 2b), created strong stratification that inhibited vertical mixing and upward nutrient enrichment to the surface layer. Surface phosphate concentrations were under detection limit, indicating limited phytoplankton growth in this region (Fig. 3m), resulting in low surface phytoplankton-C levels, which were less than 7 μg C L^{-1}.

At the equatorial region, phytoplankton-C levels were higher in the western region (>10 μg C L^{-1}) than in the eastern region (stations EQ10 and EQ12, ~7 μg C L^{-1}) (Fig. 4a). During the inter-monsoon period in spring, strong westerly winds generate the Wyrtki Jet at the Equator (Wyrtki, 1973), which can depress the thermocline and DIN nutricline, leading to associated nutrient depletion. This is consistent with the nutrient conditions observed along Section EQ in this study (Fig. 3k, o). However, a co-occurrence of DIN depletion (Fig. 3K) with a high Chl *a* value in the surface layer (Fig. 2f) was observed in the western Equator region (stations EQ01 and EQ02). The depressed thermocline and DIN isoline indicated little possibility of an upward nutrient supply to support the high phytoplankton biomass there. Strutton et al. (2015) found that high Chl *a* concentrations could be generated near the Maldivers (at 80.5°E by the RAMA mooring) by inland effects in the equatorial region, and then advected eastward by the Wyrtki Jet. Jiang et al. (2022) also found a similar phenomenon with satellite-observed Chl *a* data. These results, along with our study, suggest that phytoplankton were possibly first stimulated by nutrient enrichment in the west equatorial region and then advected eastward by the Wyrtki Jet, resulting in the relatively high phytoplankton carbon biomass observed in the western Equator region in this study.

In the southern EIO, the highest phytoplankton-C level was observed at station S10-03 (18.85 μg C L^{-1}), and phytoplankton-C levels at other stations in Section S10 also exceeded 10 μg C L^{-1}. Nutrient distributions indicated sporadic high nutrient concentration values in the surface layer along Section S10 (Fig. 2c-e). Between 10°S and 20°S in the southern EIO, the SEC transports nutrient-rich ITF water westward (Hood et al., 2017), which could support the relatively high nutrient levels and phytoplankton-C levels observed along Section S10 in the southern EIO.

4.3. The vertical distribution pattern of carbon biomass differed among the various phytoplankton groups

There is currently little information available regarding the vertical distribution pattern of carbon biomass for different phytoplankton groups in the EIO. This knowledge gap is significant as the response of phytoplankton to environmental factors such as irradiance and nutrients can differ depending on the phytoplankton group. PRO-C and SYN-C was found to demonstrate different vertical distribution pattern in this study, with SYN-C being highest in the surface layer, while PRO-C distributing homogenously in the upper 50 m layer (Fig. 8a, c). Picophytoplankton have developed various protective mechanisms to ensure their growth and survival under highly illuminated conditions, such as thermal dissipation of excess light excitation and structural changes of the photosynthetic machinery (Mella-Flores et al., 2012). Previous studies have demonstrated that PRO and SYN exhibit different responses to light stress. For instance, Six et al. (2007) found that PRO strains were more susceptible to high irradiance as compared to SYN strains in incubation experiments. Additionally, in the central Atlantic Ocean, SYN exhibited a higher resistance to irradiance than PRO in terms of cell abundance and mortality rates when exposed to varying levels of natural solar radiation (Agusti and Llabres, 2007). Thus, compared to PRO, SYN may be better adapted to the highly illuminated surface layer in the EIO, which was consistent with the distribution pattern in this study (Fig. 8a, c).

The vertical distribution pattern of PEUK-C was significantly different from that of PRO-C and SYN-C in this study, with a maximum

value found in the DCM layer (Fig. 8a-c). This observation is consistent with previous studies that also reported increasing abundances of PEUK with depth, reaching maximum values at the DCM in the Atlantic subtropical gyres (Pérez et al., 2006). The contrasting vertical distribution pattern between PEUK and the other two picophytoplankton groups (PRO and SYN) can be attributed to their distinct physiological characteristics. PEUK has been reported to have a higher tolerance to low temperatures and light levels compared with PRO and SYN, which may enable them to survive better in the DCM layer (Zubkov et al., 2000).

The carbon biomass of diatom was found to be low in the upper 50 m layers and reached a maximum in the DCM layer (Fig. 8d), related to the higher nutrient concentration at the DCM than the upper layer (Fig. 3u-x). This distribution pattern can be attributed to the fact that diatom cells have low growth rates in oligotrophic conditions but can have high growth rates under high-nutrient conditions due to their nutrient storage and surge uptake abilities (Marañón et al., 2012). For instances, large diatoms often dominate in upwelling areas with high nutrient concentrations, whereas small picophytoplankton are geographically concentrated in oligotrophic oceans between 50°N and 50°S (Irwin et al., 2006). Therefore, diatoms showed high carbon biomass in the DCM layer where elevated nutrient diffusion from below coexists with still sufficient irradiance (Beckmann and Hense, 2007). In contrast, the carbon biomass of dinoflagellates did not increase with increasing nutrient availability vertically, suggesting that this group may endure better nutrient-limiting conditions than diatoms. The homogenous vertical distribution of dinoflagellate carbon in the upper 50 m layer (Fig. 8e) is related to their mixotrophic lifestyle, which is widespread among dinoflagellate species (Jeong et al., 2010). This strategy could be advantageous in oligotrophic environments where it can supplement C fixation and nutrients for dinoflagellate cells.

4.4. C:Chl *a* of phytoplankton and its regulating factors in the EIO

Carbon-to-chlorophyll *a* ratio (C:Chl *a*) is a widely used metric for estimating phytoplankton carbon biomass from Chl *a* values in the ocean (Jakobsen and Markager, 2016). However, C:Chl *a* of phytoplankton is not a constant value and can vary from <30 to >200 g g^{-1} in the ocean (Sathyendranath et al., 2009). This variability is primarily due to phytoplankton's acclimation to various environmental conditions such as light, temperature, and nutrients (MacInture et al., 2002; Bellacicco et al., 2016), as well as variations in phytoplankton species composition (Geider et al., 1997). Most biogeochemical models utilize a constant C:Chl *a* ratio, or simply use the C:Chl *a* ratio to calculate phytoplankton carbon biomass from Chl *a* without taking into account its variability (Wang et al., 2009). Therefore, it is essential to comprehend the variation of C:Chl *a* of phytoplankton to accurately estimate regional to global primary productivity using satellite-derived Chl *a* concentrations. Several studies have reported a nonlinear relationship between phytoplankton-C and Chl *a* in the field (Sathyendranath et al., 2009; Jakobsen and Markager, 2016; Guo et al., 2021):

$$\text{Log } PC = \log A + \beta \times \log \text{Chl } a \quad (4)$$

Where *PC* is phytoplankton-C, log *A* is the intercept and β is the slope of the regression. The log-log scatter plots of phytoplankton-C vs Chl *a* of all data in this study are shown in Fig. 10. The slope (β) was 0.92, indicating that C:Chl *a* value decreased with increasing Chl *a* concentrations in the EIO.

In this study, we found that the C:Chl *a* ratio of phytoplankton in the surface layer of the EIO ranged from 20.28 to 132.16 g g^{-1}, with a mean of 70.34 ± 28.52 g g^{-1}. This range falls within the reported values in the literature (Booth et al., 1993; Wang et al., 2009; Taylor and Landry, 2018) (Table 3). Our estimate of C:Chl *a* ratio in the EIO is similar to those in other oligotrophic oceans, such as the North Pacific (20-170 g g^{-1}, Taylor and Landry, 2018) and the Kuroshio zone (94 g g^{-1}, Chang et al., 2003), but higher than those in coastal seas, such as the coastal

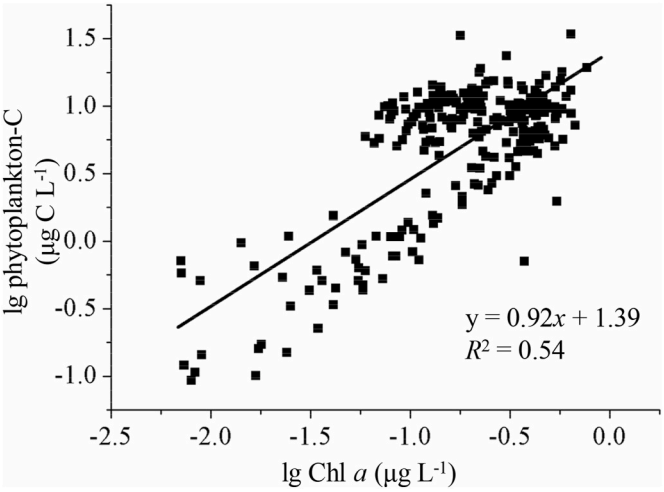

Fig. 10. Lg-lg relationship between Chl *a* (μg L^{-1}) and phytoplankton-C (μg C L^{-1}) of all data points in the EIO in this study.

East China Sea (18 g g^{-1}, Chang et al., 2003), the Jiaozhou Bay, China (31 g g^{-1}, Guo et al., 2021) and the Danish coasts (41 g g^{-1}, Jakobsen and Markager, 2016). The high C:Chl *a* ratio observed in the oligotrophic region is likely due to the high-light and low-nutrient conditions (Geider et al., 1997; Taylor et al., 1997). In nutrient-limited conditions, metabolic activities of phytoplankton cells may decrease while photosynthesis (carbon assimilation) continues (Thomas et al., 1999), leading to an increase in C:N ratio and higher C:Chl *a* ratios. Furthermore, the phytoplankton community in the EIO is dominated by PRO, which has a higher C:Chl *a* ratio than diatoms and dinoflagellates (Geider et al., 1997; Sathyendranath et al., 2009), which could also contribute to the higher C:Chl *a* ratio in this region than in the coastal seas.

This study demonstrated significant spatial variations in C:Chl *a* values of phytoplankton, which decreased with increasing water depth (Fig. 9c). The observed trend could be attributed to the variability in the light intensity and nutrient concentrations with depth (Fig. 3i-x). In the upper layer, where light intensity was higher, and nutrients concentrations were lower, C:Chl *a* values were also higher. Previous research has suggested that phytoplankton cells adapt to low light levels by increasing Chl *a* concentration per cell, which enhances light capture efficiency (Cullen, 1982; Veldhuis and Kraay, 2004; Behrenfeld et al., 2005). On the other hand, under low nutrient conditions in the upper layer, the carbon assimilation process in phytoplankton cells continues, while the nitrogen synthesis and cell division are constrained, leading to the accumulation of carbon in phytoplankton cells and higher C:Chl *a* values (Wang et al., 2009). Thus, the vertical variability in C:Chl *a* values of phytoplankton in this study could be largely explained by the variability in the irradiance and nutrient levels with depth.

4.5. DCM is not a phytoplankton-C maximum in the EIO

Since Chl *a* is commonly used to represent phytoplankton biomass, the DCM is often considered as the maximum layer in phytoplankton biomass in the EIO (Yuan et al., 2019; Jiang et al., 2022). However, several studies found that DCM may not necessarily reflect the maximum in phytoplankton biomass when considering carbon biomass as the index in stratified regions. Pérez et al. (2006) reported that phytoplankton-C concentrations were higher in the upper layers of the water column in the Atlantic subtropical gyres, while Chl *a* showed a DCM. In the oligotrophic Mediterranean Sea, Mena et al. (2019) found that phytoplankton-C maxima were located around the 25 m layer, while DCM appeared at the 75 m layer. Similarly, Gui et al. (2020) observed homogeneous distribution of phytoplankton-C in the euphotic zone of the oligotrophic slope South China Sea. These studies suggest

Table 3
Mean and range of C:Chl *a* of phytoplankton in the field and laboratory studies.

Location	Depth (m)	Phytoplankton type	C: Chl *a* range	C: Chl *a* mean ± SD	Reference
Laboratory	nd	Diatoms	21-75	39	Sathyendranath et al. (2009)
Laboratory	nd	Dinoflagellates	22-62	34	Sathyendranath et al. (2009)
Laboratory	nd	Cyanobacteria	74-126	93	Sathyendranath et al. (2009)
Laboratory	nd	*Prochlorococcus* sp.	123-126	125	Sathyendranath et al. (2009)
Coastal					
Alboran Sea	Surface		8-60	–	Arin et al. (2002)
Coastal East China Sea	2 m	Dominated by diatom	–	18	Chang et al. (2003)
Danish coasts	0-10 m	Total phytoplankton	–	41 ± 44	Jakobsen and Markager (2016)
Sagami Bay	0-50 m	Dominated by diatom	1.8-128.8	–	Ara et al. (2019)
Jiaozhou Bay, China	0.5 m	Dominated by diatom	11-62	31.6	Guo et al. (2021)
Oceanic					
North Pacific	Surface	Total phytoplankton	22-157	–	Booth et al. (1993)
Kuroshio zone	2 m	Dominated by *Trichodesmium*	–	94	Chang et al. (2003)
Atlantic Ocean	Surface		125-200	–	Veldhuis and Kraay (2004)
Equatorial Pacific Ocean	Surface	–	100-160	–	Wang et al. (2009)
North Pacific	Euphotic zone	Total phytoplankton	20-170	–	Taylor and Landry (2018)
EIO	5 m	Total phytoplankton	20-132	70 ± 29	This study

–: none data.

that the DCM might not always indicate the carbon-biomass maximum in oligotrophic oceans.

In this study, the existence of DCM is a noticeable characteristic of the vertical distribution of Chl *a* in the EIO (Fig. 3y-B), but it remains unclear whether it reflects a phytoplankton-C biomass maximum in the study area. Although Chl *a* is commonly used to estimate phytoplankton standing stock, it represents only a small portion of dry weight and organic carbon of phytoplankton cells, and the cellular Chl *a* content varies widely with the variation of taxonomic groups, growth conditions, and physiological states of phytoplankton cells (Jakobsen and Markager, 2016). Therefore, comparing the vertical distribution of phytoplankton-C with that of Chl *a* (Fig. 9a and b) indicates that, in general, the DCM was not a phytoplankton-C biomass maximum in this study. The average Chl *a* concentration at the DCM was 0.46 ± 0.13 μg L^{-1}, which was significantly higher than that (0.16 ± 0.09 μg L^{-1}) in the surface layer (*t*-test, $p < 0.01$, n = 42). A paired *t*-test revealed that no significant difference was observed for the phytoplankton-C between surface (9.56 ± 3.01 μg L^{-1}) and the DCM layer (9.07 ± 3.75 μg L^{-1}) ($p > 0.1$, n = 40). Therefore, we found little evidence to support the existence of a phytoplankton-C maximum at the DCM in this study. The average C: Chl *a* ratio was 22.07 ± 17.02 g g^{-1} at the DCM, compared with 70.34 ± 28.52 g g^{-1} in the surface layer, and these observations agree with those of Pérez et al. (2006) in the Atlantic subtropical gyres and Mena et al. (2019) in the Mediterranean Sea. Therefore, DCM may not necessarily correspond to a phytoplankton-C maximum in the EIO, but a physiological adaptation of C: Chl *a* ratios of phytoplankton cells. Vertical profiles of Chl *a* should be interpreted with caution when establishing their ecological significance in this area.

5. Conclusions

In this study, a unique data set of phytoplankton carbon biomass in the euphotic zone of the EIO was obtained by combining flow cytometry and microscopy techniques. Picophytoplankton was found to dominate the entire phytoplankton group in terms of carbon biomass, which was attributed to their ability to efficiently acquire nutrients for growth in oligotrophic conditions compared to Utermöhl phytoplankton cells. Among the various phytoplankton groups, PRO contributed the most to the total phytoplankton carbon biomass, followed by PEUK. The contribution of other phytoplankton groups was less than 20%. The spatial distribution of total phytoplankton-C showed notable variations in the EIO. Surface phytoplankton-C was relatively low in the Bay of Bengal, and relatively high values were sporadically observed in the western Equator region and the southern EIO. The observed spatial variability was mainly attributed to the physical processes in the EIO, such as the freshwater inputs in the Bay of the Bengal, Wyrtki Jet at the Equator and Southern Equatorial Current in the southern EIO. Furthermore, the vertical distribution of different phytoplankton groups showed distinct patterns in terms of carbon biomass. This variation could be attributed to their varying responses to the changes in irradiance and nutrient availability across the water column. No significant difference was observed for phytoplankton-C between the surface and DCM layers, suggesting that DCM may not correspond to a phytoplankton-C maximum in the EIO. This study sheds light on the dynamic response of phytoplankton carbon biomass to the complex physical and chemical conditions in the EIO. The findings provide valuable information for assessing carbon flows from primary producers to other trophic levels, as well as for evaluating remineralization and export production in this area.

Declaration of competing interest

The authors declare that they have no known competing financial interests or personal relationships that could have appeared to influence the work reported in this paper.

Data availability

Data will be made available on request.

Acknowledgement

The authors express their gratitude to the crew of R/V “SHIYAN 3” for their invaluable support in collecting the samples. This work was supported by the Strategic Priority Research Program of the Chinese Academy of Sciences (No. XDB42000000), the National Natural Science Foundation of China (No. 32371619), International Partnership Program of Chinese Academy of Sciences (133137KYSB20200002 and 121311KYSB20190029) and Taishan Scholar Project to Sun Song. Data and samples were collected onboard of R/V “SHIYAN 3” during the open research cruise NORC2021-10, which was supported by the NSFC Shiptime Sharing Project (project number: 42049910).

Appendix A. Supplementary data

Supplementary data to this article can be found online at https://doi.org/10.1016/j.dsr.2023.104190.

References

Agusti, S., Llabres, M., 2007. Solar radiation-induced mortality of marine pico-phytoplankton in the oligotrophic ocean. Photochem. Photobiol. 83, 793–801.

Ara, K., Fukuyama, S., Okutsu, T., Nagasaka, S., Shiomoto, A., 2019. Seasonal variability in phytoplankton carbon biomass and primary production, and their contribution to particulate carbon in the neritic area of Sagami Bay, Japan. Plankton Benthos Res 14 (4), 224–250.
Arin, L., Moran, X., Estrada, M., 2002. Phytoplankton size distribution and growth rates in the Alboran Sea (SW Mediterranean): short term variability related to mesoscale hydrodynamics. J. Plankton Res. 24, 1019–1033.
Beckmann, A., Hense, I., 2007. Beneath the surface: characteristics of oceanic ecosystems under weak mixing conditions - a theoretical investigation. Prog. Oceanogr. 75, 771–796.
Behrenfeld, M.J., Boss, E., Siegel, D.A., Shea, D.A., 2005. Carbon-based ocean productivity and phytoplankton physiology from space. Global Biogeochem. Cycles 19 (1), GB1006.
Bellacicco, M., Volpe, G., Colella, S., Pitarch, J., Santoleri, R., 2016. Influence of photoacclimation on the phytoplankton seasonal cycle in the Mediterranean Sea as seen by satellite. Remote Sens. Environ. 184, 595–604.
Blanchot, J., Rodier, M., 1996. Picophytoplankton abundance and biomass in the western tropical Pacific Ocean during the 1992 El Niño year: results from flow cytometry. Deep-Sea Res. Part II 43 (6), 877–895.
Booth, B., Lewin, J., Postel, J.R., 1993. Temporal variation in the structure of autotrophic and heterotrophic communities in the subarctic Pacific. Prog. Oceanogr. 32, 57–99.
Chang, J., Shiah, F.K., Gong, G.C., Chiang, K.P., 2003. Cross-shelf variation in carbon-to-chlorophyll *a* ratios in the East China Sea, summer 1998. Deep-Sea Res. Part II 50, 1237–1247.
Chen, Z., Gu, T., Sun, J., 2023. Disentangling environmental effects on picophytoplankton communities in the Eastern Indian Ocean. Environ. Res. 225, 115635.
Crawford, D.W., Cefarelli, A.O., Wrohan, I.A., Wyatt, S.N., Varela, D.E., 2018. Spatial patterns in abundance, taxonomic composition and carbon biomass of nano- and microphytoplankton in Subarctic and Arctic Seas. Prog. Oceanogr. 162, 132–159.
Cullen, J.J., 1982. The deep chlorophyll maximum: comparing vertical profiles of chlorophyll *a*. Can. J. Fish. Aquat. Sci. 39, 791–803.
Geider, R.J., MacIntyre, H.L., Kana, T.M., 1997. Dynamic model of phytoplankton growth and acclimation: responses of the balanced growth rate and the chlorophyll *a*: carbon ratio to light, nutrient limitation and temperature. Mar. Ecol. Prog. Ser. 148, 187–200.
Graff, J.R., Westberry, T.K., Milligan, A.J., Brown, M.B., Dall'Olmo, G., van Dongen-Vogels, V., Reifel, K.M., Behrenfeld, M.J., 2015. Analytical phytoplankton carbon measurements spanning diverse ecosystems. Deep-Sea Res., Part A I 102, 16–25.
Gui, J., Wei, Y.Q., Sun, J., Le, F.F., Cai, Y.M., Ning, X.R., 2020. Summer phytoplankton assemblages and carbon biomass in the northern south China Sea. Continent. Shelf Res. 210, 104276.
Guo, S.J., Zhao, Z.X., Liang, J.H., Du, J., Sun, X.X., 2021. Carbon biomass, carbon-to-chlorophyll *a* ratio and the growth rate of phytoplankton in Jiaozhou Bay, China. J. Oceanol. Limnol. 39 (4), 1328–1342.
Han, A.Q., Dai, M.H., Kao, S.J., Gan, J.P., Li, Q., Wang, L.F., Zhai, W.D., Wang, L., 2012. Nutrient dynamics and biological consumption in a large continental shelf system under the influence of both a river plume and coastal upwelling. Limnol. Oceanogr. 57 (2), 486–502.
Hanson, C.E., Pesant, S., Waite, A.M., Pattiaratchi, C.B., 2007. Assessing the magnitude and significance of deep chlorophyll maxima of the coastal eastern Indian Ocean. Deep-Sea Res. Part II 54, 884–901.
Harrison, P.J., Zingone, A., Mickelson, M.J., Lehtinen, S., Ramaiah, N., Kraberg, A.C., Sun, J., McQuatters-Gollop, A., Jakobsen, H.H., 2015. Cell volumes of marine phytoplankton from globally distributed coastal data sets. Estuar. Coast Shelf Sci. 162, 130–142.
Hermes, J.C., Masumoto, Y., Beal, L.M., Roxy, M.K., Vialard, J., Andres, M., Annamalai, H., Behera, S., D'Adamo, N., Doi, T., Feng, M., Han, W., Hardman-Mountford, N., Hendon, H., Hood, R., Kido, S., Lee, C., Lee, T., Lengaigne, M., Li, J., Lumpkin, R., Navaneeth, K.N., Milligan, B., McPhaden, M.J., Ravichandran, M., Shinoda, T., Singh, A., Sloyan, B., Strutton, P.G., Subramanian, A.C., Thurston, S., Tozuka, T., Ummenhofer, C.C., Unnikrishnan, A.S., Venkatesan, R., Wang, D., Wiggert, J., Yu, L., Yu, W., 2019. A sustained ocean observing system in the Indian Ocean for climate related scientific knowledge and societal needs. Front. Mar. Sci. 6, 355.
Hillebrand, H., Dürselen, C.D., Kirschtel, D., Pollingher, U., Zohary, T., 1999. Biovolume calculation for pelagic and benthic microalgae. J. Phycol. 35, 403–424.
Hodges, B.A., Rudnick, D.L., 2004. Simple models of steady deep maxima in chlorophyll and biomass. Deep-Sea Res., Part A I 51 (8), 999–1015.
Hong, L.S., Wang, C.S., Zhou, Y.D., Chen, M.R., Liu, H.B., Lin, Z.Y., Song, X.S., 2012. The distribution of chlorophyll *a* in the tropical eastern Indian Ocean in austral summer. Acta Oceanol. Sin. 31 (5), 146–159.
Hood, R.R., Beckley, L.E., Wiggert, J.D., 2017. Biogeochemical and ecological impacts of boundary currents in the Indian Ocean. Prog. Oceanogr. 156, 290–325.
Irwin, A.J., Finkel, Z.V., Schofield, O.M.E., Falkowski, P.G., 2006. Scaling-up from nutrient physiology to the size-structure of phytoplankton communities. J. Plankton Res. 28 (5), 459–471.
Jakobsen, H.H., Markager, S., 2016. Carbon-to-chlorophyll ratio for phytoplankton in temperate coastal waters: seasonal patterns and relationship to nutrients. Limnol. Oceanogr. 61 (5), 1853–1868.
Jana, S., Gangopadhyay, A., Chakraborty, A., 2015. Impact of seasonal river input on the Bay of Bengal simulation. Continent. Shelf Res. 104, 45–62.
Jeong, H.J., Yoo, Y.D., Kim, J.S., Seong, K.A., Kang, N.S., Kim, T.H., 2010. Growth, feeding and ecological roles of the mixotrophic and heterotrophic dinoflagellates in marine planktonic food webs. Ocean Sci. J. 45, 65–91.
Jiang, S.Y., Hashihama, F., Masumoto, Y., Liu, H.B., Ogawa, H., Saito, H., 2022. Phytoplankton dynamics as a response to physical events in the oligotrophic Eastern Indian Ocean. Prog. Oceanogr. 203, 102784.
MacInture, H.L., Kana, T.M., Anning, T., 2002. Photoacclimation of photosynthesis irradiance response curves and photosynthetic pigments in microalgae and cyanobacteria. J. Phycol. 38, 17–38.
Marañón, E., Cermeño, P., Latasa, M., Tadonléké, R.D., 2012. Temperature, resources, and phytoplankton size structure in the ocean. Limnol. Oceanogr. 57, 1266–1278.
Mella-Flores, D., Six, C., Ratin, M., Partensky, F., Boutte, C., Corguillé, G.L., Marie, D., Blot, N., Gourvil, P., Kolowrat, C., Garczarek, L., 2012. *Prochlorococcus* and *Synechococcus* have evolved different adaptive mechanisms to cope with light and UV stress. Front. Microbiol. 3, 285.
Mena, C., Reglero, P., Hidalgo, M., Sintes, E., Santiago, R., Martin, M., Moyà, G., Balbin, R., 2019. Phytoplankton community structure is driven by stratification in the oligotrophic Mediterranean Sea. Front. Microbiol. 10, 1698.
Menden-Deuer, S., Lessard, E.J., 2000. Carbon to volume relationships for dinoflagellates, diatoms, and other protest plankton. Limnol. Oceanogr. 45, 569–579.
Olson, R.J., Zettler, E.R., DuRand, M.D., 2018. Phytoplankton analysis using flow cytometry. In: Kemp, P.F., Cole, J.J., Sherr, B.F., Sherr, E.B. (Eds.), Handbook of Methods in Aquatic Microbial Ecology. CRC Press, Boca Raton, pp. 175–186.
Paxinos, R., Mitchell, J.G., 2000. A rapid Utermöhl method for estimating algal numbers. J. Plankton Res. 22 (12), 2255–2262.
Pérez, V., Fernández, E., Marañón, E., 2006. Vertical distribution of phytoplankton biomass production and growth in the Atlantic subtropical gyres. Deep-Sea Res., Part A I 53, 1616–1634.
Phillips, H.E., Tandon, A., Furue, R., Hood, R., Ummenhofer, C.C., Benthuysen, J.A., Menezes, V., Hu, S.J., Webber, B., Sanchez-Franks, A., Cherian, D., Shroyer, E., Feng, M., Wijesekera, H., Chatterjee, A., Yu, L., Hermes, J., Murtugudde, R., Tozuka, T., Su, D., Singh, A., Centurioni, L., Prakash, S., Wiggert, J., 2021. Progress in understanding of Indian Ocean circulation, variability, air-sea exchange, and impacts on biogeochemistry. Ocean Sci. 17 (6), 1677–1751.
Putland, J.N., Iverson, R.L., 2007. Phytoplankton biomass in a subtropical estuary: distribution, size composition, and carbon:chlorophyll ratios. Estuar. Coast 5, 1559–2723.
Ray, R.T., Haas, L.W., Sieracki, M.E., 1989. Autotrophic picoplankton dynamics in a Chesapeake Bay sub-estuary. Mar. Ecol. Prog. Ser. 52, 273–285.
Sardessai, S., Shetye, S., Maya, M.V., Mangala, K.R., Kumar, S.P., 2010. Nutrient characteristics of the water masses and their seasonal variability in the eastern equatorial Indian Ocean. Mar. Environ. Res. 70 (3–4), 272–282.
Sathyendranath, S., Stuart, V., Nair, A., Oka, K., Nakane, T., Bouman, H., Forget, M.H., Maass, H., Platt, T., 2009. Carbon-to-chlorophyll ratio and growth rate of phytoplankton in the sea. Mar. Ecol. Prog. Ser. 383, 73–84.
Six, C., Finkel, Z.V., Irwin, A.J., Campbell, D.A., 2007. Light variability illuminates niche-partitioning among marine pico-cyanobacteria. PLoS One 2, e1341.
Strutton, P.G., Coles, V.J., Hood, R.R., Matear, R.J., McPhaden, M.J., Phillips, H.E., 2015. Biogeochemical variability in the central equatorial Indian Ocean during the monsoon transition. Biogeosciences 12 (8), 2367–2382.
Sun, J., Liu, D.Y., 2003. Geometric models for calculating cell biovolume and surface area for phytoplankton. J. Plankton Res. 25 (11), 1331–1346.
Taylor, A.G., Landry, M.R., 2018. Phytoplankton biomass and size structure across trophic gradients in the southern California Current and adjacent ocean ecosystems. Mar. Ecol. Prog. Ser. 592, 1–17.
Taylor, A.H., Geider, R.J., Gilbert, F.J.H., 1997. Seasonal and latitudinal dependencies of phytoplankton carbon-to-chlorophyll *a* ratios: results of a modeling study. Mar. Ecol. Prog. Ser. 152, 51–66.
Thomas, H., Ittekkot, V., Osterroht, C., Schneider, B., 1999. Preferential recycling of nutrients—the ocean's way to increase new production and to pass nutrient limitation? Limnol. Oceanogr. 44, 1999–2004.
Veldhuis, M., Kraay, G., 2004. Phytoplankton in the subtropical Atlantic Ocean: towards a better assessment of biomass and composition. Deep-Sea Res., Part A I 51, 507–530.
Wang, J., 2017. Observational bifurcation of Wyrtki Jets and its influence on the salinity balance in the eastern Indian Ocean. Atmos. Oceanogr. Sci. Libr. 10 (1), 36–43.
Wang, X.J., Borgne, R.L., Murtugudde, R., Busalacchi, A.J., Behrenfeld, M., 2009. Spatial and temporal variability of the phytoplankton carbon to chlorophyll ratio in the equatorial Pacific: a basin-scale modeling study. J. Geophys. Res. 114, C07008.
Wang, X., Murtugudde, R., Hackert, E., Marañón, E., 2013. Phytoplankton carbon and chlorophyll distributions in the equatorial Pacific and Atlantic: a basin-scale comparative study. J. Mar. Syst. 109–110, 138–148.
Wei, Y.Q., Sun, J., Zhang, X.D., Wang, J., Huang, K., 2018. Picophytoplankton size and biomass around equatorial eastern Indian Ocean. Microbiol. 8 (2), e00629.
Wei, Y.Q., Zhang, G.C., Chen, J., Wang, J., Ding, C.L., Zhang, X.D., Sun, J., 2019. Dynamic responses of picophytoplankton to physicochemical variation in the eastern Indian Ocean. Ecol. Evol. 9, 5003–5017.
Welschmeyer, N.A., 1994. Fluorometric analysis of chlorophyll *a* in the presence of chlorophyll *b* and pheopigments. Limnol. Oceanogr. 39 (8), 1985–1992.
Wyrtki, K., 1973. An equatorial jet in the Indian Ocean. Science 181 (4096), 262–264.
Yuan, C., Xu, Z.J., Zhang, X.L., Wei, Q.S., Wang, H.W., Wang, Z.L., 2019. Photosynthetic physiologies of phytoplankton in the eastern equatorial Indian Ocean during the spring inter-monsoon. Acta Oceanol. Sin. 38, 83–91.

Yuan, C., Zhang, X.L., Wang, Z.L., Li, Y., Xu, Z.J., Wei, Q.S., Liu, L., 2021. Latitudinal distribution of the picoplankton community in the eastern equatorial Indian Ocean during the boreal fall intermonsoon period. Deep-Sea Res., Part A I 168, 103451.
Zamanillo, M., Ortega-Retuerta, E., Nunes, S., Rodríguez-Ros, P., Dall'Osto, M., Estrada, M., Sala, M.M., Simó, R., 2019. Main drivers of transparent exopolymer particle distribution across the surface Atlantic Ocean. Biogeosciences 16, 733–749.
Zubkov, M.V., Sleigh, M.A., Burkill, P.H., Leakey, R.J.G., 2000. Picoplankton community structure on the Atlantic Meridional Transect: a comparison between seasons. Prog. Oceanogr. 45 (3–4), 369–386.